Structure–function analysis of Sua5 protein reveals novel functional motifs required for the biosynthesis of the universal t^6A tRNA modification

ADELINE PICHARD-KOSTUCH,[1,3,6] WENHUA ZHANG,[1,4,6] DOMINIQUE LIGER,[1] MARIE-CLAIRE DAUGERON,[1] JULIETTE LÉTOQUART,[1,5] INES LI DE LA SIERRA-GALLAY,[1] PATRICK FORTERRE,[1,2] BRUNO COLLINET,[1] HERMAN VAN TILBEURGH,[1] and TAMARA BASTA[1]

[1]Institute for Integrative Biology of the Cell (I2BC), CEA, CNRS, Université Paris-Sud, Université Paris-Saclay, 91198, Gif-sur-Yvette cedex, France
[2]Unité de Biologie Moléculaire du Gène chez les Extrêmophiles, Département de Microbiologie, Institut Pasteur, 75014 Paris, France

ABSTRACT

N^6-threonyl-carbamoyl adenosine (t^6A) is a universal tRNA modification found at position 37, next to the anticodon, in almost all tRNAs decoding ANN codons (where N = A, U, G, or C). t^6A stabilizes the codon–anticodon interaction and hence promotes translation fidelity. The first step of the biosynthesis of t^6A, the production of threonyl-carbamoyl adenylate (TC-AMP), is catalyzed by the Sua5/TsaC family of enzymes. While TsaC is a single domain protein, Sua5 enzymes are composed of the TsaC-like domain, a linker and an extra domain called SUA5 of unknown function. In the present study, we report structure–function analysis of *Pyrococcus abyssi* Sua5 (*Pa*-Sua5). Crystallographic data revealed binding sites for bicarbonate substrate and pyrophosphate product. The linker of *Pa*-Sua5 forms a loop structure that folds into the active site gorge and closes it. Using structure-guided mutational analysis, we established that the conserved sequence motifs in the linker and the domain–domain interface are essential for the function of *Pa*-Sua5. We propose that the linker participates actively in the biosynthesis of TC-AMP by binding to ATP/PPi and by stabilizing the *N*-carboxy-L-threonine intermediate. Hence, TsaC orthologs which lack such a linker and SUA5 domain use a different mechanism for TC-AMP synthesis.

Keywords: tRNA modification; threonylcarbamoyl adenosine; t^6A_{37}; Sua5; TsaC

INTRODUCTION

To be functional in the cell, tRNA molecules need to be post-transcriptionally modified by the addition of a variety of chemical groups (Grosjean et al. 1995). One of the most complex modifications is the N^6-threonyl-carbamoyl adenosine (t^6A) is found exclusively at position 37 (3′ adjacent to anticodon) of tRNAs that decode codons of the type ANN (where N = A, U, G, or C) (Fig. 1A; Chheda et al. 1969; Takemura et al. 1969; Powers and Peterkofsky 1972). Except in some insect symbionts with highly reduced genomes, the t^6A modification is ubiquitously distributed among cellular organisms as well as in organelles such as mitochondria and chloroplasts (Machnicka et al. 2013; Boccaletto et al. 2018). t^6A prevents frameshifting during translation by stabilizing the pairing between the A_1 from the codon and the U_{36} from the anticodon (Weissenbach and Grosjean 1981; Sonawane and Sambhare 2015). In addition, its presence was reported to be critical for the binding of the anticodon stem–loop to the mRNA-ribosome complex in vitro (Stuart et al. 2000; Yarian et al. 2002; Murphy et al. 2004; Lescrinier et al. 2006; Agris 2008). Abolition of t^6A biosynthesis is lethal in *Escherichia coli* (*E. coli*) (El Yacoubi et al. 2009; Thiaville et al. 2015a). In *Saccharomyces cerevisiae* (*S. cerevisiae*), the absence of t^6A increases the occurrence of frameshifting, leaky scanning of start codons, and read-through of stop codons and leads to a dramatically reduced fitness (Lin et al. 2010; Daugeron et al. 2011; El Yacoubi et al. 2011; Thiaville et al. 2016). Recently, mutations in the

[3]**Present address: Laboratory of Biochemistry, École Supérieure de Physique et de Chimie Industrielles de la Ville de Paris (ESPCI Paris), CNRS UMR 8231, 75231 Paris Cedex 05, France**
[4]**Present address: School of Life Sciences, Lanzhou University, 730000 Lanzhou, China**
[5]**Present address: de Duve Institute and Université catholique de Louvain, 1200 Brussels, Belgium**
[6]**Joint first authors**
Corresponding authors: herman.van-tilbeurgh@i2bc.paris-saclay.fr, tamara.basta@i2bc.paris-saclay.fr
Article is online at http://www.rnajournal.org/cgi/doi/10.1261/rna.066092.118.

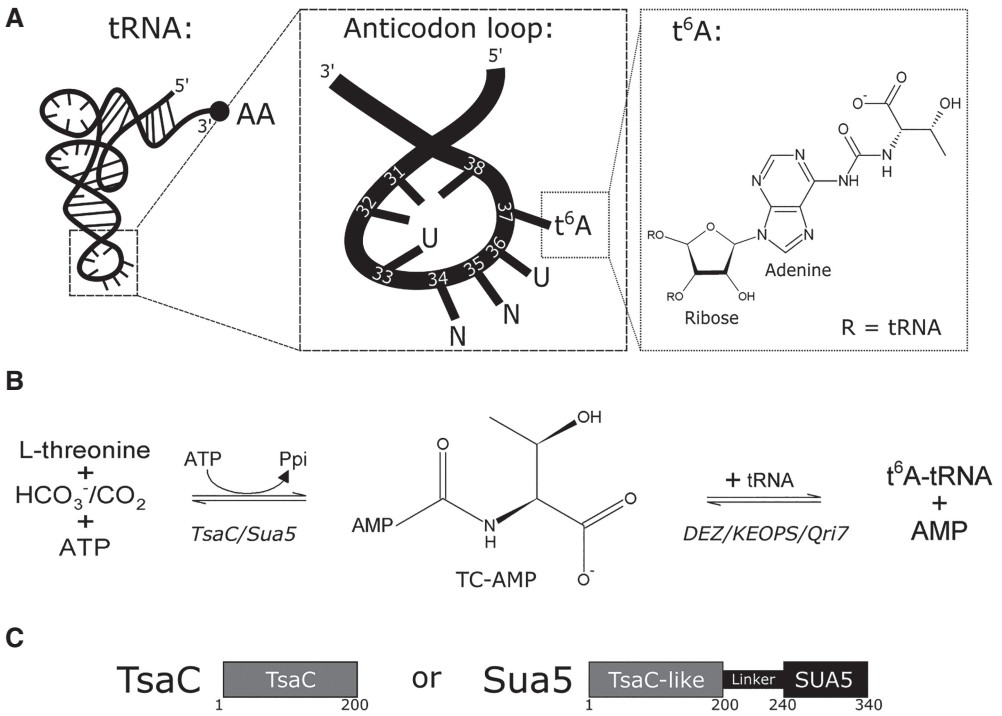

FIGURE 1. Structure and biosynthesis pathway of t^6A. (*A*) N^6-threonyl-carbamoyl adenosine (t^6A) is depicted at position 37 of the anticodon loop (enlarged) of tRNA carrying an NNU anticodon (where N = A, U, G, or C). In the absence of t^6A, the nonvariable U_{33} nucleoside can form Watson–Crick H-bonds with A_{37}, which results in a conformational change of the anticodon loop and less efficient codon–anticodon interaction. The black bars represent the orientation of the nucleoside bases relative to the phosphodiester backbone. The *right* panel shows the chemical structure of t^6A. (*B*) The t^6A biosynthesis pathway. In the first step, the conversion of L-threonine, HCO_3^-/CO_2 and ATP into L-threonyl-carbamoyl adenylate (TC-AMP) and inorganic pyrophosphate (PPi) is catalyzed by two enzyme variants: Sua5 and TsaC. In the second step, TC-AMP is used as a substrate by the KEOPS complex (in archaea and in the cytoplasm of eukaryotes), the Qri7 protein (in mitochondria), or the DEZ complex (in bacteria) which catalyze the transfer of the L-threonyl-carbamoyl moiety to A_{37} of substrate tRNA to form t^6A-tRNA and AMP. (*C*) Schematic representation of TsaC and Sua5. TsaC is a single domain protein of about 200 amino acids (in dark gray) while Sua5 consists of a TsaC-like domain connected via a linker of about 40 residues to a globular C-terminal domain of about 100 amino acids (in black).

t^6A synthetase genes were linked to a severe neurological and renal genetic disease in humans (Braun et al. 2017; Edvardson et al. 2017).

The t^6A biosynthesis reaction proceeds in two consecutive steps (Fig. 1B) catalyzed by two universal enzyme families: Sua5/TsaC* (*, previously YrdC) and Kae1/TsaD‡/Qri7 (‡, previously YgjD). Sua5/TsaC catalyzes the condensation of L-threonine, bicarbonate (HCO_3^-) or carbon dioxide (CO_2), and ATP to form inorganic pyrophosphate (PPi) and L-threonyl-carbamoyl adenylate (TC-AMP). The exact nature of the carbonaceous substrate, HCO_3^- or CO_2, is not yet unambiguously identified. The TC-AMP intermediate is taken up by Kae1/TsaD/Qri7 that transfers the L-threonyl-carbamoyl moiety onto the substrate tRNA to form t^6A-tRNA (El Yacoubi et al. 2009, 2011; Srinivasan et al. 2011; Lauhon 2012; Deutsch et al. 2012; Perrochia et al. 2013a; Wan et al. 2013). Except in mitochondria, where Qri7 works alone as a homodimer (Wan et al. 2013; Thiaville et al. 2014), Kae1/TsaD requires the presence of essential accessory proteins to be active. In bacteria, TsaD forms with two bacteria-specific proteins, TsaB (previously YeaZ) and TsaE (previously YjeE), a complex called DEZ (Deutsch et al. 2012; Lauhon 2012; Nichols et al. 2013; Zhang et al. 2015b). In archaea and in the cytoplasm of eukaryotes, Kae1 associates with Bud32, Pcc1, and Cgi121 into a complex called KEOPS or EKC (recently renamed TCTC [for nomenclature of t^6A synthetic genes, see Thiaville et al. 2014]), hereafter referred to as KEOPS for simplicity (Downey et al. 2006; Kisseleva-Romanova et al. 2006; Mao et al. 2008; Perrochia et al. 2013b; Thiaville et al. 2014; Zhang et al. 2015b). A fifth member of KEOPS, Gon7, is found exclusively in fungi and its counterpart, C14ORF142, was recently reported in humans and several other metazoans (Zhang et al. 2015a; Wan et al. 2016). The exact function of the accessory proteins of both DEZ and KEOPS complexes is unknown.

The TsaC protein from *E. coli* (*Ec*-TsaC) folds in a compact α/β twisted open-sheet structure composed of seven α helixes and seven adjacent β strands in parallel and antiparallel orientations (Teplova et al. 2000; Fu et al. 2010; Harris et al. 2015). The overall structure is reminiscent of a baseball glove with a large central concave cavity. This cavity has a positive global charge and was suggested to act as nucleic acid binding surface (Teplova et al. 2000). Indeed, *Ec*-TsaC protein binds tRNA or the anticodon arm structure with high affinity in

vitro (El Yacoubi et al. 2009; Harris et al. 2011, 2013). The active site of Sua5/TsaC is found in this cavity and involves several highly conserved residues among which is the tetrad $K^{50}xR^{52}/S^{139}xN^{141}$ (*Ec*-TsaC numbering) that plays a role in the binding of ATP and is essential for activity both in TsaC and Sua5 proteins (Teplova et al. 2000; El Yacoubi et al. 2009; Kuratani et al. 2011; Wan et al. 2013; Harris et al. 2015). The C-terminal extremity of the *Ec*-TsaC protein was shown to have an abnormally high flexibility and was proposed to be important for the enzymatic activity by acting like a gating loop (Harris et al. 2015).

Sua5 protein comprises an N-terminal TsaC-like domain and a C-terminal SUA5 domain. The two domains are connected via a linker containing about 40 residues (Fig. 1C). The structure of *Sulfolobus tokodaii* Sua5 (*St*-Sua5) was resolved in complexes with L-threonine and AMPPNP (Kuratani et al. 2011) and with TC-AMP (Agari et al. 2008; Parthier et al. 2012). The overall fold of the TsaC-like domain of *St*-Sua5 is very similar to *Ec*-TsaC while the SUA5 domain adopts a Rossmann fold (Agari et al. 2008; Kuratani et al. 2011). However, about twenty residues in the linker connecting the two domains were not resolved in the structures of *St*-Sua5.

Despite the available atomic structures of Sua5 and TsaC enzymes, the mechanism by which the Sua5/TsaC catalyze the formation of TC-AMP is not yet understood. TC-AMP is an unstable molecule with a half-life of 3.5 min under standard conditions, i.e., pH 7.5, 37°C, 2 mM $MgCl_2$ (Lauhon 2012). Decomposition of TC-AMP in aqueous media produce AMP and a nearly equimolar mixture of L-threonine and its cyclic derivate 5-methyl-2-oxazolidinone-4-carboxylate as final products (Lauhon 2012). Despite this instability, direct contact between Sua5 and Qri7 from *S. cerevisiae* is not required for in vitro t^6A synthesis, suggesting that TC-AMP is a diffusible reaction intermediate (Wan et al. 2013). Still, the exact mechanism of transfer of TC-AMP during t^6A synthesis remains to be fully elucidated. Domains homolog to TsaC are also found in the (NiFe)-hydrogenase maturation factor HypF and the *O*-carbamoyl transferases CmcH/NodU/TobZ family (Petkun et al. 2011; Parthier et al. 2012), where they catalyze carbamoylation reactions similar to those of Sua5/TsaC.

Both Sua5 and TsaC are found in the three domains of life, Archaea, Eukarya, and Bacteria, but most species encode only one of the two homologs (Thiaville et al. 2015b). For instance, *Homo sapiens* carries a TsaC protein while *S. cerevisiae* and *Plasmodium falciparum* carry a Sua5 protein. This puzzling phylogenetic repartition and the successful in vitro and in vivo complementation assays between *Ec*-TsaC and Sua5 from *S. cerevisiae* (*Sc*-Sua5) (El Yacoubi et al. 2009), as well as the lack of data concerning the SUA5 domain, hinder comprehension of the function of this domain.

To better understand the role of the interdomain linker and the SUA5 domain and to gain insight into the functional differences between TsaC and Sua5 enzymes, we performed structure–function analysis of *Pyroccocus abyssi* Sua5 (*Pa*-Sua5). We present here the crystal structure of *Pa*-Sua5, including for the first time the linker region structured between the TsaC-like and SUA5 domains. The linker is positioned in front of the catalytic cavity. Using structure-guided mutational analysis we established that conserved residues in the linker and in the SUA5 domain are essential for the TC-AMP formation. The data further suggest that the linker controls the access of the substrates/products to the active site and that tight interaction between the TsaC-like domain and SUA5 domain is required for this function. The identification of novel functional motifs specific to Sua5 proteins is an asset for further studies of the complex catalytic mechanism taking place during the biosynthesis of the universal t^6A-tRNA modification.

RESULTS

Crystallographic structure of Sua5 from *P. abyssi* reveals a novel conformation of the linker

We first determined the apo-structure of *Pa*-Sua5 at 2.8 Å resolution. The asymmetric unit contains four copies of *Pa*-Sua5 with an average root mean square deviation (RMSD) of 0.6 Å over 341 Cα atoms. The molecular mass of *Pa*-Sua5 in solution, as determined by SEC-MALLS is 38.02 kDa, which is consistent with *Pa*-Sua5 being a monomer (Supplemental Fig. S1) as reported for *St*-Sua5 (Agari et al. 2008; Kuratani et al. 2011). *Pa*-Sua5 and *St*-Sua5 share 80% sequence similarity and their overall structure is very similar, with an RMSD of 0.67 Å over 318 Cα atoms (Supplemental Fig. S2A). A residual electron density cloud at the bottom of the catalytic pocket could be fitted by a L-threonine molecule, which copurified with the enzyme. L-threonine occupies the same pocket as the threonyl moiety of TC-AMP in the *St*-Sua5 structure (Supplemental Fig. S2B,C). It forms hydrogen bonds (H-bonds) with five highly conserved residues of the catalytic domain: Thr^{35}, His^{67}, Arg^{121}, Ser^{181}, and Arg^{195} (Supplemental Fig. S2B). Atop the active site, two H_2O molecules (Supplemental Fig. S3B) are bound tightly via H-bonds with the conserved residues Arg^{58}, Asn^{62}, and His^{234} for one and Arg^{58} and Ser^{147} for the other.

The main difference between the structures of *Pa*-Sua5 and of *St*-Sua5 resides in the linker peptide connecting the TsaC-like and the SUA5 domains (Supplemental Fig. S2A). This region is partly disordered in the *St*-Sua5 structures, respectively from Pro^{215} to Lys^{233} (*St*-Sua5 numbering) for the TC-AMP bound form (PDB: 4E1B) and from Glu^{216} to Lys^{236} for the AMPPNP bound form (PDB: 3AJE). In *Pa*-Sua5, the linker is fully ordered (Fig. 2A), starting with one short α-helical turn from Pro^{215} to Tyr^{218}, followed by a twisted hairpin from Asp^{223} to Lys^{231} that enters the active site pocket and continues by a ω-loop that folds up against the active site cavity before joining the SUA5 domain. This

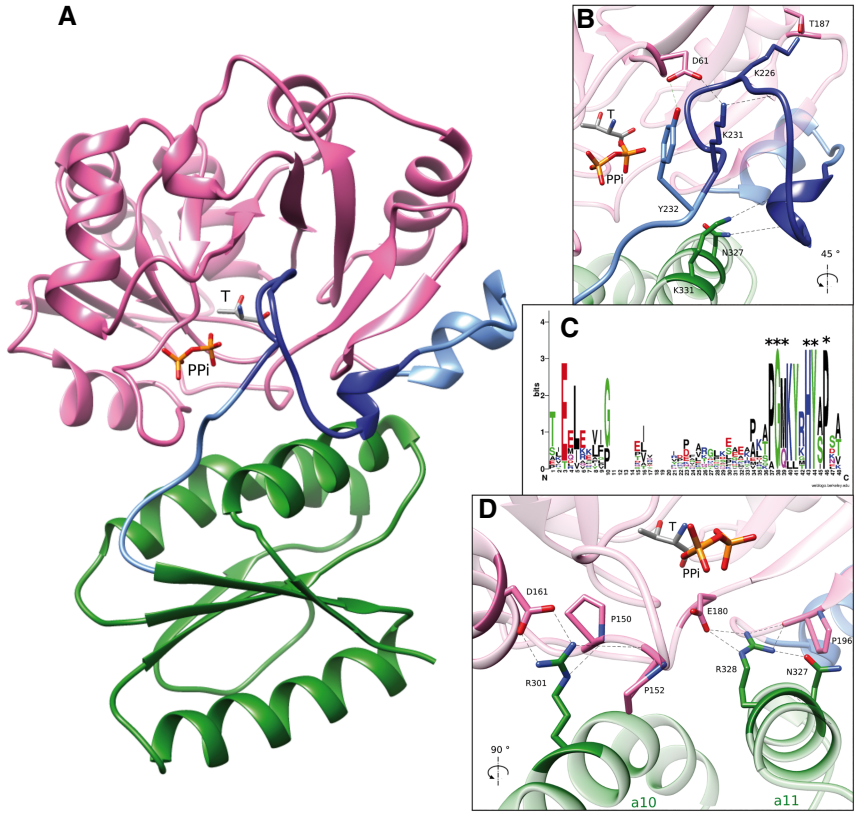

FIGURE 2. The structure of *Pa*-Sua5. (*A*) The overall structure of *Pa*-Sua5 bound to PPi and L-threonine (denoted as T). The TsaC-like domain (in pink) is similar to the *Ec*-TsaC structures (PDB: 1HRU and 2MX1). The SUA5 domain (in green) is a Rossmann fold. The linker (in blue) is fully ordered in the *Pa*-Sua5 structures. The region that is missing in *St*-Sua5 structures is colored in dark blue. (*B*) Zoomed-in view of the active site of *Pa*-Sua5. H-bonds between the linker and conserved core residues of both the TsaC-like and the SUA5 domains are indicated as black dashed lines. Regions apart from the linker and the residues involved in its stabilization are shown as transparent. (*C*) Conservation of the linker (residues 200–239 in *Pa*-Sua5). The multiple sequence alignment was done with 13 Sua5 sequences (five archaea, five bacteria, and three eukaryotes) using MAFFT. Results were depicted using Weblogo (Crooks et al. 2004). The asterisks indicate the residues of the motifs Pro^{228}–Gly^{229}–Met^{230} and His^{234}–Tyr^{235} that were targeted by mutagenesis. (*D*) Zoomed-in view of the interdomain surface of *Pa*-Sua5. The conserved residues Arg^{301} and Arg^{328} interact with several residues of the TsaC-like domain that are highly conserved in Sua5 proteins.

linker conformation is stabilized by several interactions involving conserved residues (Fig. 2B). The α-helical turn is stabilized through H-bonds between the backbone of Ala^{216} and Val^{217} and the amine functions of, respectively, Lys^{331} and Asn^{327} in the SUA5 domain. The hairpin is stabilized through interaction between Lys^{226} and the residue Thr^{187} in the TsaC-like domain. Lys^{231} forms H-bonds with Asp^{61} in the TsaC-like domain and with the backbone of Asp^{223}. Finally, Tyr^{232} forms H-bonds with Asp^{61}.

To map the substrate/product binding sites of *Pa*-Sua5, we cocrystallized the protein with ATP, L-threonine, HCO_3^- and $MgCl_2$. Crystals were obtained in the same conditions as for the L-threonine bound form and diffracted at 2.6 Å. The asymmetric unit contains four copies of *Pa*-Sua5 with an average RMSD of 0.53 Å over 340 Cα atoms. There was no indication for bound nucleotides, but we observed residual electron density in the active site cavity, which could be satisfactorily fitted by a PPi ion and an L-threonine (Fig. 2A). L-threonine occupies the same position in both *Pa*-Sua5 structures (Supplemental Figs. S3A, S4C,D). PPi was likely generated by the hydrolysis of ATP during the crystallization and displaces two water molecules present in the L-threonine bound structure (Supplemental Fig. S3C). PPi is bound at the periphery of the active site where it occupies a positively charged electrostatic surface potential patch (Supplemental Fig. S3D). The oxygens of the phospho-moieties are coordinated by H-bonds respectively with Arg^{58}, Asn^{62}, and Gly^{229} and with Lys^{56}, Arg^{58}, Ser^{147}, Gly^{148}, and His^{234} (Supplemental Fig. S3C). These are all highly conserved residues and Gly^{229} and His^{234} belong to the linker (Supplemental Fig. S3C). This is a distinctive feature of Sua5 proteins because the TsaC proteins have no linker. Lys^{56}, Arg^{58}, and Ser^{143} belong to the conserved tetrade K^{56}xR^{58}/S^{143}xN^{145} (*Pa*-Sua5 numbering), shown to be essential for ATP binding. PPi does not occupy exactly the same position as the β- and γ-phosphate groups of AMPPNP in *St*-Sua5 (Supplemental Fig. S4B,D), but it clashes with the β phosphate of AMPPNP and with the phospho-moiety of TC-AMP (Fig. 3C). This suggests that the presence of PPi in the active site of *Pa*-Sua5 may compete with binding of a nucleotide. It was shown that YrdC is capable of catalyzing the reverse reaction at high concentrations of PPi (Lauhon 2012). The TC-moiety of TC-AMP is oriented in a different direction compared to the β- and γ-phosphate groups of AMPPNP, and PPi is ideally positioned for the reverse nucleophilic attack of the phosphate of TC-AMP, yielding ATP.

The linker is superposable in both *Pa*-Sua5 structures, indicating that PPi is not required for its structuration (Supplemental Fig. S3A). The linker hangs over the active site gorge, blocking its access (Fig. 3A). The adenylate parts of AMPPNP and TC-AMP occupy the same position in the *St*-Sua5 structures (Supplemental Fig. S4A,B). Structure superposition of *Pa*-Sua5 with *St*-Sua5 reveals a clash between the linker hairpin residues Lys^{226}-Ala^{227}-Pro^{228} and the adenyl-moiety of both AMPPNP and TC-AMP (Fig. 3C). This conformation of the linker is therefore not compatible with the presence of a nucleotide in the active site. In *Pa*-Sua5, the conserved His^{234} of the linker binds to PPi while

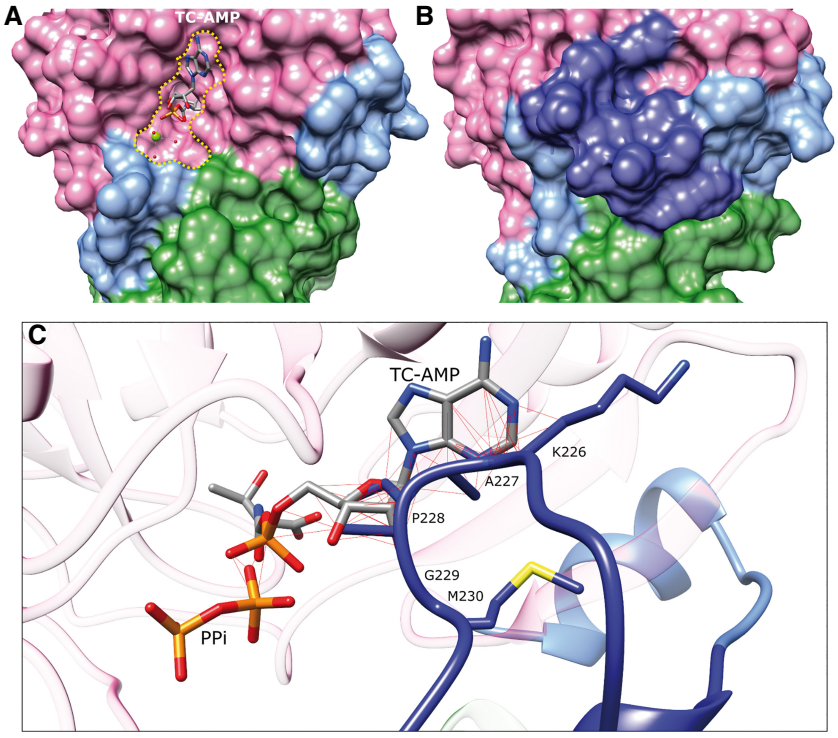

FIGURE 3. Linker acts as a lid closing the active site pocket of Sua5 proteins. (*A*) Surface representation of *St*-Sua5 bound to TC-AMP (PDB: 4E1B). The active site pocket is bordered by yellow dots. The surface of the structured part of the linker is colored in blue. (*B*) Surface representation of *Pa*-Sua5. The peptide of the linker that becomes ordered is in dark blue. The linker completely closes the active site. (*C*) Superposition of *St*-Sua5 bound to TC-AMP and *Pa*-Sua5 bound to PPi. Ligands and the side chains of the linker are indicated in color while the *Pa*-Sua5 protein main chain is shown as transparent. Main chain of *St*-Sua5 is not shown. Clashes between the linker hairpin residues and the adenyl-moiety of TC-AMP and between PPi and the phospho-moiety of TC-AMP are shown by red lines. Clashes were determined using UCSF Chimera (Pettersen et al. 2004).

in the TC-AMP bound form of *St*-Sua5, its side chain points toward the solvent (Supplemental Fig. S4). Similarly, the side chain of the neighboring residue Tyr^{235} is oriented deeper in the active site in the AMPPNP *St*-Sua5 structure, forming a H-bond with the β phosphate of AMPPNP and the Ser^{144} of the KxR/SxN tetrade (Supplemental Fig. S4B). The binding of ATP and/or TC-AMP may thus be regulated via these two linker residues. A highly conserved proline, Pro^{237}, is found next to the bend of the linker C-terminal extremity (Supplemental Fig. S4).

The *Pa*-SUA5 domain adopts a Rossmann fold with an inner β sheet composed of five strands and framed by three α helices. Helices α10 (Val^{289} to Arg^{305}) and α11 (Gly^{320} to Ser^{333}) form a typical α/α coil, interacting via a hydrophobic zipper formed by the conserved Leu^{296}, Leu^{300}, Val^{325}, and Leu^{329}. Several conserved residues of α10 and α11 form a network of noncovalent interactions with residues from the catalytic domain conserved among Sua5 proteins. Notably, Arg^{301} forms H-bonds with the side-chain of Asp^{161} and with the Pro^{150} and Pro^{152} backbones and, in a similar way, Arg^{328} interacts with Glu^{180} and Pro^{196} (Fig. 2C). Arg^{301} and Arg^{328} are like two arms holding together the two domains of Sua5-proteins.

In vitro kinetics of ATP hydrolysis by *Pa*-Sua5^{wt}

Sua5/TsaC proteins require L-threonine, ATP, and HCO_3^-/CO_2 to synthesize TC-AMP and PPi via a complex mechanism that involves the formation of two covalent bonds (Agari et al. 2008; El Yacoubi et al. 2009; Lauhon 2012; Harris et al. 2015). The precise reaction mechanism of the enzymes is still unknown. As an initial step toward the elucidation of the catalytic mechanism of *Pa*-Sua5^{wt}, we determined the kinetic constants for the hydrolysis reaction of ATP into AMP. We used a radioactive assay to measure the initial velocity of the reaction at varying concentrations of either L-threonine or ATP. The concentration of HCO_3^-/CO_2 was constant as it is always present in solution if no precautions are undertaken. The best nonlinear least squares fit of the data produced a hyperbolic curve for both substrates, indicating that the reaction obeys the classical Michaelis–Menten kinetics (Supplemental Fig. S5). We found K_m and k_{cat} values of 11.5 ± 1.3 μM and 0.054 ± 0.002 sec^{-1} for L-threonine, and 5.5 ± 1.3 μM and 0.029 ± 0.001 sec^{-1} for ATP. The unexpected difference in k_{cat} values may be a consequence of large variations in quantification of radioactive AMP at low ATP concentrations (Supplemental Fig. S5B). Our data are comparable to the apparent rate constants for the ATPase activity of *St*-Sua5 of 0.04 and 0.1 sec^{-1} at 37 and 60°C, respectively, in the presence of 1 mM ATP, 5 mM $MgCl_2$, 50 mM K-HEPES pH 7.5, and 100 mM KCl (Agari et al. 2008).

The TsaC-like domain of *Pa*-Sua5 is highly unstable in the absence of the SUA5 domain

The structures of the catalytic domains of *Ec*-TsaC and of *Pa*- and *St*-Sua5 enzymes are very similar. To find out if the SUA5 domain is required for TC-AMP synthesis, we tested truncated variants of *Pa*-Sua5. We made three constructs: *Pa*-Sua5$^{\Delta(240–340)}$ and *Pa*-Sua5$^{\Delta(200–340)}$ correspond to the TsaC-like domain, respectively with or without the linker; *Pa*-Sua5$^{\Delta(1–239)}$ corresponds to the SUA5 domain. After expression in *E. coli*, *Pa*-Sua5$^{\Delta(200–340)}$ and *Pa*-Sua5$^{\Delta(240–340)}$ could not be detected by Coomassie staining in the soluble fraction, and *Pa*-Sua5$^{\Delta(1–239)}$ was significantly less soluble

than *Pa*-Sua5^{wt} under different expression conditions tested (see Materials and Methods). Still, small amounts of *Pa*-Sua5$^{\Delta(200–340)}$, *Pa*-Sua5$^{\Delta(240–340)}$, and *Pa*-Sua5$^{\Delta(1–239)}$ could be obtained in soluble and pure form but none of them exhibited detectable ATPase activity in vitro (data not shown). We noticed that these truncated proteins were rapidly degraded under several storage conditions tested, indicating that they are highly unstable. Linker and SUA5 domains thus appear to be essential for the stability of the TsaC-like domain of *Pa*-Sua5.

Mutations in the conserved residues of the linker and SUA5 domain produce stable proteins

The structure of *Pa*-Sua5 suggests that the linker and the SUA5 domain could interfere with enzymatic activity. We set out to test this hypothesis by mutating several conserved residues in the linker and at the domain interface. The sequence conservation score of each residue was calculated using 500 orthologs and mapped onto the *Pa*-Sua5 structure using Consurf (Supplemental Fig. S6; Ashkenazy et al. 2016). The linker region from Ala^{225} to Ala^{239}, facing the active site, contains several highly conserved residues. Notably the motifs Pro^{228}–Gly^{229}–Met^{230} (Fig. 3C) and His^{234}–Tyr^{235} (Supplemental Fig. S4) are positioned, respectively, near the adenyl-moiety and the phosphate groups of PPi/ATP. To test the importance of these motifs for the activity, we generated the *Pa*-Sua5$^{P228A/G229A/M230A}$ and *Pa*-Sua5$^{H234A/Y235A}$ mutants. We also tested the *Pa*-Sua5^{P237A} and *Pa*-Sua5^{P237S} mutants, reasoning that this strictly conserved proline could influence the flexibility of the linker region. In addition, we constructed the *Pa*-Sua5$^{R301A/R328A}$ and *Pa*-Sua5$^{R301D/R328D}$ mutants to test if the integrity of the domain interface affects the activity of Sua5 proteins.

We first evaluated the effect of the mutations on protein stability using gel filtration experiments and DSC analysis (Supplemental Fig. S7). The gel filtration elution profiles of the mutant proteins were similar to that of the wild-type protein, indicating that the mutations did not modify significantly the Stokes radius of *Pa*-Sua5 (Supplemental Fig. S7A). The DSC analysis produced single relatively narrow and symmetric peaks for all proteins corresponding to a highly cooperative unfolding process typical for compact globular proteins (Supplemental Fig. S7B). The sharp drop at the end of the curve indicated a nonreversible denaturation for all proteins. *Pa*-Sua5^{wt} has a melting temperature of 80.8 ± 0.3°C in agreement with the hyperthermophilic nature of *P. abyssi*. The linker mutants *Pa*-Sua5$^{P228A/G229A/M230A}$, *Pa*-Sua5$^{H234A/Y235A}$, *Pa*-Sua5^{P237A}, and *Pa*-Sua5^{P237S} unfolded over a temperature range similar to that of *Pa*-Sua5^{wt} (75°C–85°C), with no major impact on melting temperatures (78.85°C–80.86°C). In contrast, the endothermic peaks recorded for Pa-Sua5$^{R301A/R328A}$ and Pa-Sua5$^{R301D/R328D}$ were broader and their melting temperatures were 5°C lower, suggesting that mutations of the interdomain interface affect the stability of *Pa*-Sua5.

The conserved residues in the linker and SUA5 domain are functionally important

We used in vivo complementation assays in *S. cerevisiae* to test if the above-identified residues are functionally important. The absence of the *SUA5* gene in yeast results in an extremely slow growth phenotype. Thus, we used as host a *S. cerevisiae* strain that carried chromosomal deletion of the *SUA5* gene and a plasmid YcpLac33 expressing the endogenous *SUA5* gene in *trans*. The genes encoding mutant *Pa*-Sua5 proteins were then introduced on a second plasmid pESC-LEU. Plasmid shuffling, i.e., selection of the strain which lost the YcpLac33-*SUA5* plasmid, was done in restrictive condition by addition of 5-FOA into the growth medium. For all constructs, the presence of the pESC-LEU plasmid and the loss of the YcpLac33-*SUA5* plasmid after plasmid shuffling were validated by colony PCR (Supplemental Fig. S8A). In addition, the heterologous expression of all recombinant *Pa*-Sua5 proteins in yeast cells was confirmed using western blot (Supplemental Fig. S8B). After plasmid shuffling, *Pa*-Sua5^{wt} robustly complemented the absence of *Sc*-SUA5 even though the incubation temperature (28°C) was much below the optimal growth temperature of *P. abyssi* (96°C) (Fig. 4). A similar phenotype was observed for *Pa*-Sua5^{P237A}, but only partial growth complementation was observed for *Pa*-Sua5$^{H234A/Y235A}$, *Pa*-Sua5^{P237S}, *Pa*-Sua5$^{R301A/R328A}$, and *Pa*-Sua5$^{R301D/R328D}$. Of note, the Sua5$^{R301D/R328D}$ mutant was more affected than the *Pa*-Sua5$^{R301A/R328A}$ mutant. Expression of the *Pa*-Sua5$^{P228A/G229A/M230A}$ mutant resulted in an amorphic phenotype (similar to that of Δ*sua5* strain), indicating that this mutant has no significant activity. Together, the data indicate that the conserved residues in the linker and in the SUA5 domain are functionally important in vivo.

We next measured the in vitro ATPase activity of the *Pa*-Sua5 mutants corresponding to the amount of AMP detected after 1 h of incubation at 50°C (Fig. 5, black bars). The activities of the *Pa*-Sua5^{P237A} and *Pa*-Sua5^{P237S} mutants were similar to that of *Pa*-Sua5^{wt}. These data are in line with the in vivo data and suggest that the strictly conserved Pro^{237} at the base of the linker is not essential for the function in the conditions tested. Interestingly, *Pa*-Sua5$^{H234A/Y235A}$, *Pa*-Sua5$^{R301A/R328A}$, and *Pa*-Sua5$^{R301D/R328D}$, which partially complemented the yeast growth phenotype, were totally inactive in vitro, suggesting that the activity of these mutants can be rescued in vivo. Combined with the in vivo hypomorphic and amorphic phenotypes of these mutations, this indicates that both the His^{234}–Tyr^{235} motif and the interface residues Arg^{301} and Arg^{328} are important for *Pa*-Sua5 function. In contrast, *Pa*-Sua5$^{P228A/G229A/M230A}$ still exhibited significant ATPase activity (an approximate threefold decrease of AMP production as compared to *Pa*-Sua5^{wt}) even though it did not complement the growth of yeast. This suggests that *Pa*-Sua5$^{P228A/G229A/M230A}$ does not produce enough TC-AMP to sustain growth or that the

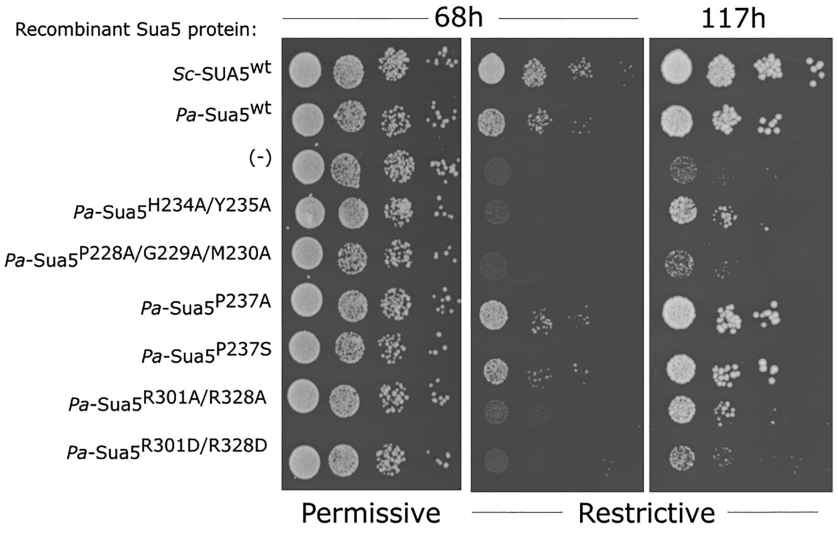

FIGURE 4. Functional complementation of Δ*sua5 S. cerevisiae* strain by recombinant *Pa*-Sua5 proteins. The function of the *Pa*-Sua5 mutant alleles was tested in a complementation assay of a Δ*sua5 S. cerevisiae* strain carrying a *URA3*-plasmid expressing *SUA5* in *trans*. pESC-LEU plasmids carrying *Pa*-Sua5 alleles under the control of the strong inducible yeast promoters pGAL1 or pGAL10 were transformed into the yeast strain. Transformants were grown in GAL−LEU medium, and serial dilutions of the cultures were spotted in parallel on GAL−LEU (permissive) and GAL−LEU + 5FOA (restrictive) plates and incubated at 28°C to monitor the complementation. The control experiment under permissive conditions (*left* panel) showed that all the constructs grew similarly.

observed in vitro production of AMP does not lead to synthesis of TC-AMP.

Effect of the presence of *Pa*-KEOPS on *Pa*-Sua5 in vitro ATPase activity

Sua5 proteins together with the KEOPS complex constitute the t^6A pathway in Eukarya and Archaea. To test whether KEOPS influences the activity of Sua5, we added in our ATPase assay the *Pa*-KEOPS complex together with cognate substrate *Pa*-$tRNA^{Lys(UUU)}$, creating reaction conditions that allow the synthesis of t^6A-tRNA. The quantity of AMP produced by *Pa*-$Sua5^{wt}$ increased approximately twofold in the presence of KEOPS alone or with tRNA but remained unaffected in the presence of BSA (Supplemental Fig. S10). *Pa*-$Sua5^{P237A}$ and *Pa*-$Sua5^{P237S}$ mutants also showed a small but significant increase of activity (P-value < 0.005) (Fig. 5, white bars). Unexpectedly, a significant amount of AMP was detected for the inactive mutants *Pa*-$Sua5^{H234A/Y235A}$, *Pa*-$Sua5^{R301A/R328A}$, and *Pa*-$Sua5^{R301D/R328D}$, respectively at 10%, 14%, and 11% of the wild-type level. In contrast, the quantity of AMP produced by *Pa*-$Sua5^{P228A/G229A/M230A}$ was not affected by the presence of KEOPS and/or tRNA. We verified indirectly whether the AMP detected corresponded to actual production of TC-AMP by measuring the t^6A-tRNA produced in the same reaction conditions. No significant amounts of t^6A could be detected for *Pa*-$Sua5^{H234A/Y235A}$, *Pa*-$Sua5^{P228A/G229A/M230A}$, *Pa*-$Sua5^{R301A/R328A}$, and *Pa*-$Sua5^{R301D/R328D}$ (Fig. 6). This suggests that these mutants hydrolyze ATP but do not form TC-AMP. The mechanisms behind the stimulating effect of KEOPS and its absence in the case of the *Pa*-$Sua5^{P228A/G229A/M230A}$ mutant remain unknown.

Crystallographic structure of *Pa*-$Sua5^{H234A/Y235A}$

The mutant *Pa*-$Sua5^{H234A/Y235A}$ was co-crystallized with ATP, L-threonine, HCO_3^- and $MgCl_2$ in the same conditions as for *Pa*-$Sua5^{wt}$. Crystals belonged also to the C2 space group but with different cell edges from the crystals of the wild-type protein. Data were obtained at a

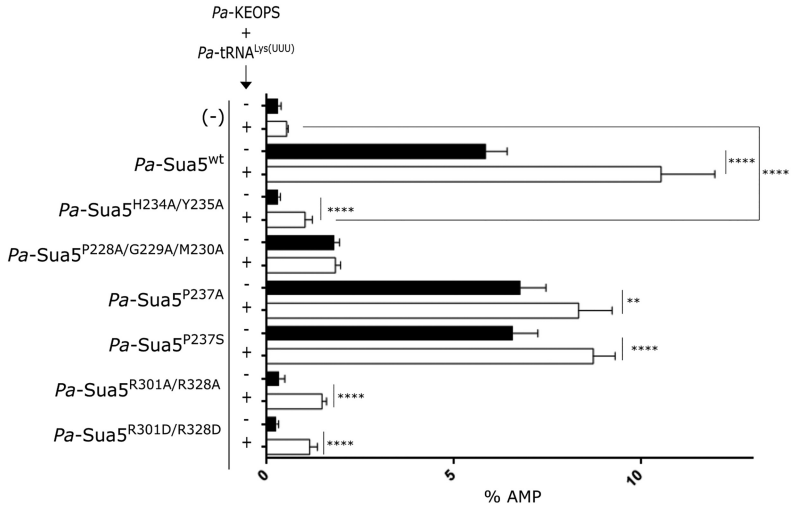

FIGURE 5. In vitro ATPase activity of *Pa*-Sua5 proteins. ATPase activity assays were performed using 2 µM of *Pa*-Sua5 enzymes. Where indicated, the mixture was incubated in the presence of *Pa*-KEOPS at 2 µM and *Pa*-$tRNA^{Lys(UUU)}$ at 5 µM (white bars). After incubation for 1 h at 50°C in the presence of radioactive [α^{32}-P] ATP, the nucleotides were separated using TLC (see Supplemental Fig. S10 and Materials and Methods section). Radioactive spots corresponding to ATP and AMP were recorded and quantified. All experiments were done at least in technical triplicates and biological duplicate. The bars correspond to standard error deviation. The data were analyzed using a *t*-test (P-value < 0.05). Significant differences are indicated by (****), where P-value < 0.0001 and (**), where P-value < 0.01.

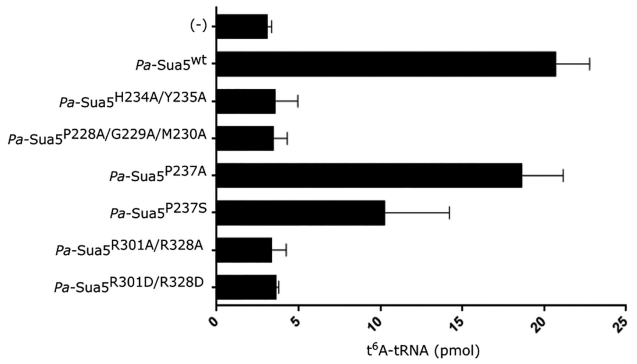

FIGURE 6. In vitro t^6A synthesis activity of *Pa*-Sua5 proteins. t^6A activity assays were performed using 2 µM of *Pa*-Sua5 and *Pa*-KEOPS, 5 µM of *Pa*-$tRNA^{Lys(UUU)}$ and in the presence of 182 µM L-[1-^{14}C]-threonine. The reaction mixtures were incubated for 1 h at 50°C. The reactions were stopped on ice, and macromolecules were precipitated by addition of 15% TCA. tRNA was recovered on filters, and the amount of radioactive tRNA, corresponding to L-[1-^{14}C]-t^6A-tRNA, was determined by scintillation counting. All experiments were done at least in technical triplicates and biological duplicate. The bars correspond to standard deviation. The signal in the negative control sample corresponds to background noise.

resolution of 2.8 Å. The asymmetric unit contains two copies of *Pa*-$Sua5^{H234A/Y235A}$. The overall structure of *Pa*-$Sua5^{H234A/Y235A}$ is almost identical to that of *Pa*-$Sua5^{wt}$ with an RMSD of 0.54 Å over 332 Cα atoms for monomer A and of 0.55 Å over 311 Cα atoms for monomer B. The linker was clearly defined up to residue 233 in one copy of *Pa*-Sua5 but the two mutated residues were disordered. The linker is completely disordered in the second copy of *Pa*-Sua5. The structured linker region superposes well with the *Pa*-$Sua5^{wt}$ linker and is probably stabilized by crystal contacts. Although no ATP, TC-AMP, or PPi could be detected in the residual electron density, L-threonine and an electronic density cloud that could be fitted by a HCO_3^- ion were present in the active site (Supplemental Fig. S11). The HCO_3^- ion is facing the nitrogen from L-threonine (C–N distance is 3.4 Å), which occupies the same position as in all other Sua5 structures. HCO_3^- ion is stabilized by ionic interactions with Arg^{195} and the backbone of Ser^{143}, both conserved in Sua5/TsaC proteins (Supplemental Fig. S11B). The HCO_3^- ion superposes with the carbamoyl group of the TC-AMP reaction product in the *St*-Sua5 structure.

DISCUSSION

The first step of the t^6A-tRNA reaction pathway consists in the formation of the highly unstable TC-AMP (Lauhon 2012), catalyzed by two related enzymes, TsaC or Sua5. Both share an orthologous catalytic domain, but Sua5 proteins have an extra C-terminal SUA5 domain with no attributed function so far. The SUA5 domain adopts a Rossmann fold, but it is lacking residues involved in nucleotide binding (Agari et al. 2008; Kuratani et al. 2011; Parthier et al. 2012). We could not detect any in vitro ATPase activity for the SUA5 domain alone. We noticed that the SUA5 domain has no significant sequence conservation, except for residues involved in the interaction with the TsaC-like domain and a motif ^{326}MNRLXKAS^{333} at the C terminus (Supplemental Fig. S6) found in the α11. Mutations disrupting this interaction in Sua5 from *P. abyssi* provoked a significant loss in activity, indicating that the integrity of this interface is important for enzyme activity.

The linker between the two domains is partly disordered in the *St*-Sua5 structures while it has a well-defined electron density in our *Pa*-Sua5 structures. Notably, the residues from Asp^{223} to Lys^{231} form a twisted hairpin that enters the active site and overlaps with the position of AMPPNP or TC-AMP in the *St*-Sua5 structures (Fig. 3C). This conformation of the linker is also observed in the absence of bound PPi (Supplemental Fig. S3). The linker completely closes the active site, preventing binding of nucleotides (Fig. 3B). We propose that the linker acts as a lid that undergoes conformational changes during the reaction cycle, controlling the access of substrates/products to the active site.

Closure of the active site by surface loops is a recurrent mechanism used by enzymes to create favorable reaction conditions. Although this scenario is plausible for Sua5, it is not clear how TsaC catalyzes the same reaction without a linker and a SUA5 domain. In the case of *Ec*-TsaC, it was reported that the last 20 residues are flexible and that their conformation is affected by ATP binding (Teplova et al. 2000; Harris et al. 2015). This prompted Harris and colleagues to hypothesize that the C terminus acts as a flexible arm that may participate in the binding of ATP (Harris et al. 2015). It is therefore tempting to speculate that the C-terminal part of TsaC and the linker of Sua5 play similar roles.

The enzyme TobZ catalyzes the *O*-carbamoylation of the antibiotic tobramycine. The structure of TobZ from *Streptoalloteichus tenebrarius* (PDB: 3VEZ) is composed of an N-terminal Kae1/TsaD/Qri7-like domain and a C-terminal TsaC-like domain (Supplemental Fig. S12B; Parthier et al. 2012). Both domains interact closely, creating a wide internal tunnel that connects their respective active sites. The TsaC-like domain catalyzes the formation of carbamoyl-AMP using carbamoyl-phosphate and ATP as substrates. Carbamoyl-phosphate is dephosphorylated and the carbamoyl group performs a nucleophilic attack upon the α-phosphate of ATP, giving PPi and carbamoyl-AMP. Interestingly, the region between Val^{490} and Thr^{497} acts as a gating loop that closes the active site of the TsaC-like domain after ATP binding (Supplemental Fig. S12). Parthier et al. (2012) proposed that the synthesis of carbamoyl-AMP by TobZ proceeds through substrate-assisted catalysis. This hypothesis is motivated by the fact that no clear catalytic side chains are present near the carbamoyl moiety of the substrate. Similarly, TsaC/Sua5 proteins lack obvious catalytic side chains in the substrate binding site, suggesting that they also use substrate-assisted catalysis for the formation of TC-AMP.

After crystallization of *Pa*-Sua5 with all substrates such that TC-AMP can be formed, only L-threonine and PPi were bound to the active site. The formation of TC-AMP is energetically unfavorable (Lauhon 2012); even small concentrations (nM) of PPi present in the crystallization liquid would convert the TC-AMP back to ATP, which may explain why only PPi and L-threonine were found in the binding pocket. The binding site of L-threonine is deeply buried and not accessible when nucleotide analogs are occupying the active site. Therefore L-threonine and HCO_3^-/CO_2 should bind before ATP. In *Ec*-TsaC, L-threonine also must bind first to allow the correct coordination of ATP in the binding pocket (Harris et al. 2015). In *Pa*-Sua5, PPi interacts with the conserved motif His^{234}–Tyr^{235} from the linker (Supplemental Fig. S4). Mutation of this motif is important for TC-AMP synthesis, likely by playing a role in the binding of ATP and/or PPi. In our structure, PPi partially overlaps with the position of the β-phosphate moiety of the nucleotide compounds in *St*-Sua5 AMPPNP and TC-AMP complexes, suggesting that PPi may be an inhibitor of Sua5 (Fig. 3C). In agreement with this hypothesis, Lauhon (2012) observed that the TC-AMP synthesis activity of Sua5 from *Bacillus subtilis* is strongly activated in the presence of pyrophosphatase, an enzyme that hydrolyzes PPi into phosphate.

In the current view, the Sua5/TsaC enzymes synthesize an N-carboxy-L-threonine intermediate from HCO_3^-/CO_2 and L-threonine. Subsequently, N-carboxy-L-threonine attacks the α-phosphate of ATP to generate TC-AMP and PPi (Lauhon 2012; Perrochia et al. 2013a). However, this putative mechanism has not yet been demonstrated. Unexpectedly, the residual electron density of the *Pa*-$Sua5^{H234A/Y235A}$ mutant revealed the presence of a bicarbonate (HCO_3^-) in front of the L-threonine (Supplemental Fig. S11). The NH_2 group of L-threonine is directed toward the HCO_3^- ion and this likely presents the Michaelis-complex preceding the synthesis of N-carboxy-L-threonine.

The conserved Pro^{228}–Gly^{229}–Met^{230} motif is part of the hairpin that blocks the active site cavity. The *Pa*-$Sua5^{P228A/G229A/M230A}$ mutant hydrolyzes ATP, but it does not complement SUA5 deletion in vivo, nor does it produce t^6A in vitro, suggesting it is not capable of TC-AMP synthesis. This mutation could influence the conformation of the linker and may therefore affect the synthesis of N-carboxy-L-threonine and binding of ATP. We therefore propose the following mechanistic model for TC-AMP synthesis by Sua5 proteins. L-threonine and HCO_3^-/CO_2 bind first to the narrow cavity at the bottom of the active site. The linker lid likely subsequently closes the active site favoring the synthesis and stabilization of N-carboxy-L-threonine by excluding solvent and increasing the local concentration of the substrates. The subsequent opening of the lid allows ATP binding followed by nucleophilic attack of the carboxyl group of N-carboxy-L-threonine leading to TC-AMP and PPi.

In conclusion, we identified two novel binding sites in Sua5 proteins: one for the bicarbonate substrate and one for the PPi product. The structure and the functional properties of the linker suggest it plays an active role during the reaction cycle, probably related to the stabilization/synthesis of the N-carboxy-L-threonine intermediate and to the binding of ATP/PPi. The absence of linker and SUA5 domain in the TsaC proteins demonstrates that these proteins use different mechanisms to synthetize TC-AMP. TsaC and Sua5 are therefore closely related but functionally distinct orthologs. The identified functional differences provide clues to help understand the complex evolutionary history of these universal proteins.

MATERIALS AND METHODS

Cloning procedures and mutagenesis

The recombinant plasmid pET26b(+)-PAB1302-$(wt)^{6H}$ (Perrochia et al. 2013a) was used as template for site-directed mutagenesis. The mutants were constructed using Phusion polymerase (Thermo Fisher). The oligonucleotides used were synthetized (Genewiz) and are listed in Supplemental Table S1. For generating point mutations, the QuickChange Kit II (Thermofisher) protocol was used. For construction of truncated proteins, the sequences encoding for the isolated protein domains were amplified using PCR. A hexahistidine tag or a Strep-tag II was added in 5′ or 3′ of the gene, which was subsequently cloned in pET26b(+) vector (Novagen) using NdeI/XhoI restriction sites. The sequences of the constructs are available on request. Recombinant plasmids were introduced into chemocompetent *E. coli* strain TOP10 (Invitrogen). The recombinant plasmid used for heterologous expression of KEOPS complex of *P. abyssi* was previously described (Perrochia et al. 2013a).

Recombinant gene expression and protein purification

Recombinant genes were expressed in *E. coli* strains Rosetta2 (DE3) pLysS (Novagen) or XL1 GOLD (Stratagene). Protein overproduction was done in Auto Induction Media Terrific Broth Base including trace elements (Formedium) prepared according to manufacturer's protocol. Cells were collected by centrifugation, resuspended in lysis buffer 50 mM Tris-HCl pH 8, 200 mM NaCl, 10% glycerol. Lysozyme (0.1 mg/mL final) and anti-protease Roche cOmplete ULTRA tablets EDTA-free were added. Cell suspension was homogenized using the high-pressure cell disrupter One Shot (Constant Systems Ltd). After centrifugation at 30,000*g* for 30 min, the supernatant was heated at 65°C for 30 min, except for the truncated mutants, to precipitate bacterial proteins. Protein precipitate was removed by centrifugation at 30,000*g* for 60 min. His-tagged proteins from the soluble fraction were purified on a HisTrap HP using an AKTA FPLC system (GE Healthcare). Strep-tagged proteins from the soluble fraction were purified on Strep-Tactin resin (Qiagen). Fractions of interest were pooled and injected on the Superdex 75 HiLoad 16/60 (or 10/300) (GE Healthcare). Fractions containing pure proteins were concentrated, flash-frozen in liquid nitrogen, and stored at −80°C in lysis buffer containing 10%–20% of glycerol. To increase the solubility of *Pa*-Sua5 truncated mutants we (i) used classical LB media and started induction with 0.5–1 mM IPTG for 1–2 h at OD_{600} 0.6, (ii) applied a heat-shock at 42°C before induction to induce chaperon

expression, (iii) grew our cultures at 16°C and 22°C, (iv) varied purification buffers between pH 7 and 8.5 with 200–500 mM NaCl and 0%–20% glycerol. To preserve the stability of the purified proteins, storage conditions at 4°C, −20°C, and −80°C in buffer with glycerol between 10% and 30% were tested.

tRNA substrate production and purification

The template sequences for in vitro transcription were synthetized and cloned between HindIII and EcoRI restriction sites in pUC18 vector (GeneScript). The gene coding the *Pa*-tRNA$^{Lys(UUU)}$ is surrounded by two sequences coding hammerhead ribozyme in 5′ and glmS ribozyme followed by a BbsI site in 3′ (Price et al. 1995; Batey and Kieft 2007). Plasmids were linearized by the restriction endonuclease BbsI overnight at 37°C. T7 RNA polymerase was purified as previously described (Grodberg and Dunn 1988). Transcription assays contained 80 mM Na-HEPES pH 7.5, 2 mM spermidine, 40 mM DTT, 20 mM $MgCl_2$, 2.5 mM NTP, 200 µg of linearized plasmid, 31 µg/mL T7 RNA polymerase in a 10 mL reaction volume. The reaction was continued for 1 h at 37°C. The hammerhead ribozyme cleavage occurs simultaneously during the transcription. The precipitated magnesium PPi is pelleted by centrifugation at 10,000*g* for 10 min. The glmS ribozyme cleavage is performed by incubating the supernatant with 1 mM glucosamine-6-phosphate for 5 min at room temperature. The reaction was heated at 80°C for 10 min, to inactivate the enzyme, then centrifuged at 10,000*g* for 10 min. The supernatant was injected on a MonoQ 5 mL column using an AKTA FPLC system (GE Healthcare). The elution was performed by a gradient of NaCl from 0.3 mM to 1 M in 50 mM Na-HEPES pH 7.5, 5mM $MgCl_2$. After analysis on a 12% (w/v) polyacrylamide gel containing 8 M urea, the fractions containing the pure tRNA were pooled, ethanol precipitated, and solubilized in 50 mM Na-HEPES pH 7.5, 5mM $MgCl_2$. The samples were stored at −20°C.

Differential scanning calorimetry (DSC)

DSC experiments were performed using a VP-DSC calorimeter (MicroCal). *Pa*-Sua5 proteins were used at a concentration around 13 µM in 50 mM K-HEPES pH 8, and 35 mM KCl. Scanning from 20°C to 100°C at a heating speed of 1°C/min was done for each experiment. Data were analyzed using the MicroCal Origin software provided by the manufacturer.

Size-exclusion-chromatography coupled with multi-angle laser light scattering

The molecular weight of the wild-type *Pa*-Sua5 was determined using size exclusion chromatography coupled to multi-angle laser light scattering (SEC-MALLS) with the SEC-TDA equipment (Malvern). The Superdex 200 (75) HR 10/300 columns (GE Healthcare) or Bio-SEC3 column (Agilent) for SEC were equilibrated with buffer containing 20 mM Tris-HCl pH 7.5, 200 mM NaCl, and 5 mM 2-β-mercaptoethanol. Eighty microliters of *Pa*-Sua5 at a concentration of 5 mg/mL were injected at a flow rate of 0.5 mL min^{-1} onto the SEC column and eluted with the equilibration buffer at a flow rate of 0.3 mL min^{-1}. Elution was followed by a UV–visible spectrophotometer, a differential refractometer, a 7° and a 90° angle light scattering detector and a differential pressure viscometer. The OmniSEC software program was used for the acquisition and analysis of the data. BSA was used as standard reference protein of known molecular weight, concentration, refractive index increment ($dn/dc = 0.185$ mL·g^{-1}), and intrinsic viscosity to calibrate the instrument.

Crystallization, data acquisition, and structure determination

Pa-Sua5 at a final concentration of 9 mg/mL was either crystallized alone or cocrystallized with ATP/$MgCl_2$/L-threonine/HCO_3^- (all ligands were added at 5 mM) by the sitting-drop vapor diffusion method. Crystals were obtained within 3 d from a crystallization reservoir containing 0.1 M Tris pH 8.5–8.8, 3.5 M ammonium sulfate. Crystals were cryo-protected in crystallization reservoir solution supplemented with 30% glycerol and flash-frozen in liquid nitrogen. The X-ray diffraction data were collected at 100K at the Soleil Synchrotron Light Source on the Proxima 1 beam line (wavelength 0.98011 Å, PILATUS 6M detector). The images were successfully processed and scaled with the XDS package (Kabsch 2010). The data processing and refinement statistics are summarized in Supplemental Table S2. The structure was solved by molecular replacement with the program MOLREP implemented in the CCP4 suite (Winn et al. 2011) using the structure of *St*-Sua5 as the search model (PDB code: 2EQA). The model building was carried out with the program Coot (Emsley and Cowtan 2004), and the structure refinement was performed with Refmac5 (Winn et al. 2003).

Sequence alignment and structure comparison

The sequence conservation was analyzed using the program ConSurf (Ashkenazy et al. 2016) with the structure of *Pa*-Sua5 as query. Based on the default criteria, the program used CS-BLAST to identify the 500 closest homologs by BLOSOM-60 on the Uniref-90 Protein database and aligned them using MAFFT. The conservation rate of each position was calculated with Bayesian algorithms using the 150 homologous sequences with the lowest *E*-value and mapped on the structure of *Pa*-Sua5. The PDB codes of the structures are 1HRU and 2MX1 for *Ec*-TsaC, 2EQA, 3AJE, and 4E1B for *St*-Sua5, 3VEZ for *St*-TobZ. The structural comparison and the graphic representations of the protein structures were produced with UCSF Chimera (Pettersen et al. 2004). The electrostatic potential representation was rendered and produced using APBS and PDB2PQR (Unni et al. 2011). The ligands' coordination was analyzed with LigPlot+ (Laskowski and Swindells 2011).

In vitro assay for the synthesis of t^6A-modified tRNA

The reaction was performed using *Pa*-KEOPS and *Pa*-Sua5 proteins (2 µM each), purified *Pa*-tRNA$^{Lys(UUU)}$ (5 µM) in reaction buffer composed of 50 mM K-HEPES pH 8, 35 mM KCl, 10 mM $MgCl_2$, 1 mM $MnCl_2$, 5 mM DTT, 1 mM ATP, 10 mM $NaHCO_3^-$, supplemented with 182 µM L-[1-^{14}C]-threonine (0.05 µCi, 55 Ci/mol) (American Radiolabeled Chemicals). After incubation at 50°C for 1 h, macromolecules were precipitated by addition of 1 mL of Trichloroacetic acid (TCA) 15% and incubated on ice for 1 h. Precipitated material was applied on glass microfiber filters GF/F

(Whatmann), prewet with TCA 15%, using a vacuum apparatus (Millipore). Assay tubes were rinsed with 1 mL of TCA 15%, and filters were washed three times with 1 mL of TCA 5% and three times with 1 mL of ethanol 95%. After extensive drying, filters were placed into scintillation vials and soaked with 3 mL of Emulsifier Safe scintillation cocktail (Zinsser Analytic). Radioactivity was recorded as average counts per minute (CPM) during 5 min, with a Packard Liquid Scintillation Analyzer.

In vitro ATP hydrolysis assay

The ATP hydrolysis reactions (conversion into AMP and PPi) were carried out using *Pa*-Sua5 (1 or 2 μM) and, when indicated, with *Pa*-KEOPS (2 μM) and *Pa*-$tRNA^{Lys(UUU)}$ (5 μM) in the same reaction mixture as for the t^6A assay, supplemented with [α^{32}-P] ATP (3 Ci/μmol) (PerkinElmer). The reaction was performed at 50°C and stopped on ice. Radioactive nucleotides were separated by thin layer chromatography (TLC) using 0.4 M $KH_2PO_4^-$(pH 3.4) as mobile phase. One microliter of the mix was spotted on a 10×10 cm PEI-Cellulose plates (Merck), prerun in distilled water. Plates were dried and radioactivity was revealed by phosphorimaging using the scanner Typhoon Trio (GE Healthcare) (Supplemental Fig. S9). Quantification was done with ImageQuantTL software.

For the determination of enzymatic constants, L-threonine and cold ATP were added at different concentrations (3–150 μM and 5–500 μM) to measure the initial velocity of ATP hydrolysis. The enzymes were added to the final concentration of 1 or 2 μM. The reaction was performed with an incubation time up to 6 min for L-threonine titration and up to 8 min for ATP titration. We could not detect any significant background of ATPase activity in the absence of enzymes. The data were then fitted using nonlinear least squares regression applied to the Morrison or Michaelis–Menten equation using Graphpad Prism. Both equations gave very similar catalytic constant values (Supplemental Fig. S5). All the experiments were performed at least in quadruplicates.

Functional complementation assay in *S. cerevisiae* cells

Yeast cells were grown at 28°C in standard rich medium YEPD (1% yeast extract, 2% peptone, 2% glucose) or selective minimal media minus leucine with 2% galactose (GAL-LEU) or glucose (GLU-LEU) (Sigma or Euromedex). Cells were transformed using the lithium acetate method (Gietz and Schiestl 2007).

For the construction of the YcpLac33-*SUA5* plasmid, the wild-type *SUA5* gene was amplified by PCR using genomic DNA from strain BY496 as template (see Supplemental Table S1 for oligonucleotide sequences). The insert was cloned into the YcpLac33 vector using SalI/SacI restriction sites. The resulting construct was introduced in the Δ*sua5::KanMX* strain, derived from the W303 reference strain. The genes encoding wild-type and point mutant *Pa*-Sua5 proteins were amplified by PCR using the recombinant pET26b(+) plasmids (Cloning Procedures section) as templates. The PCR products were cloned into pESC-LEU vector between BglII/SacI or BamHI/SalI, and the genes were expressed under the control of respectively pGAL10 promoters, producing FLAG-tagged proteins, or pGAL1 promoters, producing myc-tagged proteins. The Δ*sua5::KanMX*–(YcpLac33-*SUA5*) strain was transformed with the recombinant pESC-LEU vectors and the transformants were selected on GLU-LEU. For each construction, three transformed clones were selected and grown on GLU-LEU. Cells were serially diluted and spotted in parallel on GAL-LEU to induce the plasmid driven expression of *Pa*-Sua5 variants and on GAL-LEU supplemented with 1 g/L^{-1} 5-fluoroorotic acid (5-FOA) to counter select YcpLac33-*SUA5* plasmid. The plates were incubated at 28°C for the time indicated in the main text.

Colony PCR

To validate the genetic constructions, several colonies per clone were selected from the GAL-LEU 5-FOA plates and suspended in 20 to 60 μL NaOH 20 mM. After incubation at 95°C for 45 min and 300 rpm, the extract was centrifuged at 11,000*g* for 10 min to remove cell debris. Supernatant was diluted and used with the adequate primers for PCR reaction using Phusion (Thermo Fisher). PCR products were sequenced for validation (Eurofins).

Western blot

Protein extraction was done using the standard protocol as previously described (Liger et al. 2011) for FLAG-tagged proteins or the Kushnirov extraction method (Kushnirov 2000) for myc-tagged proteins. Proteins from soluble fractions were resolved by SDS-PAGE on a 15% gel and transferred onto Protran nitrocellulose membrane (Whatman). Detection of myc-tagged proteins was performed using mouse 9E10 anti-myc as primary antibody (1/3000 dilution, Sigma-Aldrich) and goat anti-mouse HRP-conjugated IgG as secondary antibody (1/5000 dilution) (Sigma-Aldrich). Detection of FLAG-tagged proteins was performed using mouse anti-FLAG M2-peroxidase (HRP) (1/10 000 dilution) (Sigma-Aldrich). Immunoblots were revealed using ECL kit SuperSignal West Pico Chemiluminescent Substrate (Thermo Fisher).

DATA DEPOSITION

Atomic coordinates and structure factors for the reported crystal structures have been deposited with the Protein Data bank under accession numbers 6F89, 6F87, and 6F8Y.

SUPPLEMENTAL MATERIAL

Supplemental material is available for this article.

ACKNOWLEDGMENTS

We thank Domenico Libri for the generous gift of the *S. cerevisiae* (Δ*sua5*::Kan) strain. We thank Marc Graille for his assistance in the crystallographic data collection and analysis. This work has benefited from the platform and expertise of the Macromolecular interactions measurements Platform of I2BC. This work received support from the French Infrastructure for Structural Biology (Agence Nationale de la Recherche; FRISBI ANR-10-INSB-0501) to H.v.T. and by Lidex BIG grant of the Paris-Saclay University to T.B.L. and H.v.T. A.P.K. received her PhD scholarship from IDEX Paris-Saclay.

Received February 8, 2018; accepted April 10, 2018.

REFERENCES

Agari Y, Sato S, Wakamatsu T, Bessho Y, Ebihara A, Yokoyama S, Kuramitsu S, Shinkai A. 2008. X-ray crystal structure of a hypothetical Sua5 protein from Sulfolobus tokodaii strain 7. *Proteins* **70:** 1108–1111.

Agris PF. 2008. Bringing order to translation: the contributions of transfer RNA anticodon-domain modifications. *EMBO Rep* **9:** 629–635.

Ashkenazy H, Abadi S, Martz E, Chay O, Mayrose I, Pupko T, Ben-Tal N. 2016. ConSurf 2016: an improved methodology to estimate and visualize evolutionary conservation in macromolecules. *Nucleic Acids Res* **44:** W344–W350.

Batey RT, Kieft JS. 2007. Improved native affinity purification of RNA. *RNA* **13:** 1384–1389.

Boccaletto P, Machnicka MA, Purta E, Piatkowski P, Baginski B, Wirecki TK, de Crécy-Lagard V, Ross R, Limbach PA, Kotter A, et al. 2018. MODOMICS: a database of RNA modification pathways. 2017 update. *Nucleic Acids Res* **46:** D303–D307.

Braun DA, Rao J, Mollet G, Schapiro D, Daugeron M-C, Tan W, Gribouval O, Boyer O, Revy P, Jobst-Schwan T, et al. 2017. Mutations in KEOPS-complex genes cause nephrotic syndrome with primary microcephaly. *Nat Genet* **49:** 1529–1538.

Chheda GB, Hall RH, Mozejko J, Magrath DI, Schweizer MP, Stasiuk L, Taylor PR. 1969. Aminoacyl nucleosides. VI. Isolation and preliminary characterization of threonyladenine derivatives from transfer ribonucleic acid. *Biochemistry* **8:** 3278–3282.

Crooks GE, Hon G, Chandonia J-M, Brenner SE. 2004. WebLogo: a sequence logo generator. *Genome Res* **14:** 1188–1190.

Daugeron M-C, Lenstra TL, Frizzarin M, El Yacoubi B, Liu X, Baudin-Baillieu A, Lijnzaad P, Decourty L, Saveanu C, Jacquier A, et al. 2011. Gcn4 misregulation reveals a direct role for the evolutionary conserved EKC/KEOPS in the t^6A modification of tRNAs. *Nucleic Acids Res* **39:** 6148–6160.

Deutsch C, El Yacoubi B, de Crécy-Lagard V, Iwata-Reuyl D. 2012. Biosynthesis of threonylcarbamoyl adenosine (t^6A), a universal tRNA nucleoside. *J Biol Chem* **287:** 13666–13673.

Downey M, Houlsworth R, Maringele L, Rollie A, Brehme M, Galicia S, Guillard S, Partington M, Zubko MK, Krogan NJ, et al. 2006. A genome-wide screen identifies the evolutionarily conserved KEOPS complex as a telomere regulator. *Cell* **124:** 1155–1168.

Edvardson S, Prunetti L, Arraf A, Haas D, Bacusmo JM, Hu JF, Ta-Shma A, Dedon PC, de Crécy-Lagard V, Elpeleg O. 2017. tRNA N^6-adenosine threonylcarbamoyltransferase defect due to KAE1/TCS3 (OSGEP) mutation manifest by neurodegeneration and renal tubulopathy. *Eur J Hum Genet* **25:** 545–551.

El Yacoubi B, Lyons B, Cruz Y, Reddy R, Nordin B, Agnelli F, Williamson JR, Schimmel P, Swairjo MA, de Crécy-Lagard V. 2009. The universal YrdC/Sua5 family is required for the formation of threonylcarbamoyladenosine in tRNA. *Nucleic Acids Res* **37:** 2894–2909.

El Yacoubi B, Hatin I, Deutsch C, Kahveci T, Rousset J-P, Iwata-Reuyl D, Murzin AG, de Crécy-Lagard V. 2011. A role for the universal Kae1/Qri7/YgjD (COG0533) family in tRNA modification. *EMBO J* **30:** 882–893.

Emsley P, Cowtan K. 2004. Coot: model-building tools for molecular graphics. *Acta Crystallogr D Biol Crystallogr* **60:** 2126–2132.

Fu TM, Liu X, Li L, Su XD. 2010. The structure of the hypothetical protein smu.1377c from *Streptococcus mutans* suggests a role in tRNA modification. *Acta Crystallogr Sect F Struct Biol Cryst Commun* **66:** 771–775.

Gietz RD, Schiestl RH. 2007. Large-scale high-efficiency yeast transformation using the LiAc/SS carrier DNA/PEG method. *Nat Protoc* **2:** 38–41.

Grodberg J, Dunn JJ. 1988. ompT encodes the *Escherichia coli* outer membrane protease that cleaves T7 RNA polymerase during purification. *J Bacteriol* **170:** 1245–1253.

Grosjean H, Sprinzl M, Steinberg S. 1995. Posttranscriptionally modified nucleosides in transfer RNA: their locations and frequencies. *Biochimie* **77:** 139–141.

Harris KA, Jones V, Bilbille Y, Swairjo MA, Agris PF. 2011. YrdC exhibits properties expected of a subunit for a tRNA threonylcarbamoyl transferase. *RNA* **17:** 1678–1687.

Harris KA, Shekhtman A, Agris PF. 2013. Specific RNA-protein interactions detected with saturation transfer difference NMR. *RNA Biol* **10:** 1307–1311.

Harris KA, Bobay BG, Sarachan KL, Sims AF, Bilbille Y, Deutsch C, Iwata-Reuyl D, Agris PF. 2015. NMR-based structural analysis of threonylcarbamoyl-AMP synthase and its substrate interactions. *J Biol Chem* **290:** 20032–20043.

Kabsch W. 2010. XDS. *Acta Crystallogr D Biol Crystallogr* **66:** 125–132.

Kisseleva-Romanova E, Lopreiato R, Baudin-Baillieu A, Rousselle J-C, Ilan L, Hofmann K, Namane A, Mann C, Libri D. 2006. Yeast homolog of a cancer-testis antigen defines a new transcription complex. *EMBO J* **25:** 3576–3585.

Kuratani M, Kasai T, Akasaka R, Higashijima K, Terada T, Kigawa T, Shinkai A, Bessho Y, Yokoyama S. 2011. Crystal structure of *Sulfolobus tokodaii* Sua5 complexed with L-threonine and AMPPNP. *Proteins* **79:** 2065–2075.

Kushnirov VV. 2000. Rapid and reliable protein extraction from yeast. *Yeast* **16:** 857–860.

Laskowski RA, Swindells MB. 2011. LigPlot+: multiple ligand-protein interaction diagrams for drug discovery. *J Chem Inf Model* **51:** 2778–2786.

Lauhon CT. 2012. Mechanism of N^6-threonylcarbamoyladenonsine (t^6A) biosynthesis: isolation and characterization of the intermediate threonylcarbamoyl-AMP. *Biochemistry* **51:** 8950–8963.

Lescrinier E, Nauwelaerts K, Zanier K, Poesen K, Sattler M, Herdewijn P. 2006. The naturally occurring N^6-threonyl adenine in anticodon loop of *Schizosaccharomyces pombe* tRNAi causes formation of a unique U-turn motif. *Nucleic Acids Res* **34:** 2878–2886.

Liger D, Mora L, Lazar N, Figaro S, Henri J, Scrima N, Buckingham RH, van Tilbeurgh H, Heurgue-Hamard V, Graille M. 2011. Mechanism of activation of methyltransferases involved in translation by the Trm112 "hub" protein. *Nucleic Acids Res* **39:** 6249–6259.

Lin CA, Ellis SR, True HL. 2010. The Sua5 protein is essential for normal translational regulation in yeast. *Mol Cell Biol* **30:** 354–363.

Machnicka MA, Milanowska K, Osman Oglou O, Purta E, Kurkowska M, Olchowik A, Januszewski W, Kalinowski S, Dunin-Horkawicz S, Rother KM, et al. 2013. MODOMICS: a database of RNA modification pathways—2013 update. *Nucleic Acids Res* **41:** D262–D267.

Mao DYL, Neculai D, Downey M, Orlicky S, Haffani YZ, Ceccarelli DF, Ho JSL, Szilard RK, Zhang W, Ho CS, et al. 2008. Atomic structure of the KEOPS complex: an ancient protein kinase-containing molecular machine. *Mol Cell* **32:** 259–275.

Murphy FV, Ramakrishnan V, Malkiewicz A, Agris PF. 2004. The role of modifications in codon discrimination by $tRNA^{Lys}UUU$. *Nat Struct Mol Biol* **11:** 1186–1191.

Nichols CE, Lamb HK, Thompson P, El Omari K, Lockyer M, Charles I, Hawkins AR, Stammers DK. 2013. Crystal structure of the dimer of two essential *Salmonella typhimurium* proteins, YgjD & YeaZ and calorimetric evidence for the formation of a ternary YgjD–YeaZ–YjeE complex. *Protein Sci* **22:** 628–640.

Parthier C, Görlich S, Jaenecke F, Breithaupt C, Bräuer U, Fandrich U, Clausnitzer D, Wehmeier UF, Böttcher C, Scheel D, et al. 2012. The O-carbamoyltransferase TobZ catalyzes an ancient enzymatic reaction. *Angew Chem Int Ed Engl* **51:** 4046–4052.

Perrochia L, Crozat E, Hecker A, Zhang W, Bareille J, Collinet B, van Tilbeurgh H, Forterre P, Basta T. 2013a. *In vitro* biosynthesis of a universal t^6A tRNA modification in Archaea and Eukarya. *Nucleic Acids Res* **41:** 1953–1964.

Perrochia L, Guetta D, Hecker A, Forterre P, Basta T. 2013b. Functional assignment of KEOPS/EKC complex subunits in the biosynthesis of the universal t^6A tRNA modification. *Nucleic Acids Res* **41:** 9484–9499.

Petkun S, Shi R, Li Y, Asinas A, Munger C, Zhang L, Waclawek M, Soboh B, Sawers RG, Cygler M. 2011. Structure of hydrogenase

maturation protein HypF with reaction intermediates shows two active sites. *Structure* **19:** 1773–1783.

Pettersen EF, Goddard TD, Huang CC, Couch GS, Greenblatt DM, Meng EC, Ferrin TE. 2004. UCSF Chimera—a visualization system for exploratory research and analysis. *J Comput Chem* **25:** 1605–1612.

Powers DM, Peterkofsky A. 1972. Biosynthesis and specific labeling of N-(purin-6-ylcarbamoyl)threonine of *Escherichia coli* transfer RNA. *Biochem Biophys Res Commun* **46:** 831–838.

Price SR, Ito N, Oubridge C, Avis JM, Nagai K. 1995. Crystallization of RNA-protein complexes. I. Methods for the large-scale preparation of RNA suitable for crystallographic studies. *J Mol Biol* **249:** 398–408.

Sonawane KD, Sambhare SB. 2015. The influence of hypermodified nucleosides lysidine and t^6A to recognize the AUA codon instead of AUG: a molecular dynamics simulation study. *Integr Biol (Camb)* **7:** 1387–1395.

Srinivasan M, Mehta P, Yu Y, Prugar E, Koonin EV, Karzai AW, Sternglanz R. 2011. The highly conserved KEOPS/EKC complex is essential for a universal tRNA modification, t^6A. *EMBO J* **30:** 873–881.

Stuart JW, Gdaniec Z, Guenther R, Marszalek M, Sochacka E, Malkiewicz A, Agris PF. 2000. Functional anticodon architecture of human $tRNA^{Lys3}$ includes disruption of intraloop hydrogen bonding by the naturally occurring amino acid modification, t^6A. *Biochemistry* **39:** 13396–13404.

Takemura S, Murakami M, Miyazaki M. 1969. Nucleotide sequence of isoleucine transfer RNA from *Torulopsis utilis*. *J Biochem* **65:** 489–491.

Teplova M, Tereshko V, Sanishvili R, Joachimiak A, Bushueva T, Anderson WF, Egli M. 2000. The structure of the *yrdC* gene product from *Escherichia coli* reveals a new fold and suggests a role in RNA binding. *Protein Sci* **9:** 2557–2566.

Thiaville PC, El Yacoubi B, Perrochia L, Hecker A, Prigent M, Thiaville JJ, Forterre P, Namy O, Basta T, de Crécy-Lagard V. 2014. Cross kingdom functional conservation of the core universally conserved threonylcarbamoyladenosine tRNA synthesis enzymes. *Eukaryot Cell* **13:** 1222–1231.

Thiaville PC, El Yacoubi B, Köhrer C, Thiaville JJ, Deutsch C, Iwata-Reuyl D, Bacusmo JM, Armengaud J, Bessho Y, Wetzel C, et al. 2015a. Essentiality of threonylcarbamoyladenosine (t^6A), a universal tRNA modification, in bacteria. *Mol Microbiol* **98:** 1199–1221.

Thiaville PC, Iwata-Reuyl D, de Crécy-Lagard V. 2015b. Diversity of the biosynthesis pathway for threonylcarbamoyladenosine (t^6A), a universal modification of tRNA. *RNA Biol* **11:** 1529–1539.

Thiaville PC, Legendre R, Rojas-Benítez D, Baudin-Baillieu A, Hatin I, Chalancon G, Glavic A, Namy O, de Crécy-Lagard V. 2016. Global translational impacts of the loss of the tRNA modification t^6A in yeast. *Microb Cell* **3:** 29–45.

Unni S, Huang Y, Hanson RM, Tobias M, Krishnan S, Li WW, Nielsen JE, Baker NA. 2011. Web servers and services for electrostatics calculations with APBS and PDB2PQR. *J Comput Chem* **32:** 1488–1491.

Wan LCK, Mao DYL, Neculai D, Strecker J, Chiovitti D, Kurinov I, Poda G, Thevakumaran N, Yuan F, Szilard RK, et al. 2013. Reconstitution and characterization of eukaryotic N^6-threonylcarbamoylation of tRNA using a minimal enzyme system. *Nucleic Acids Res* **41:** 6332–6346.

Wan LCK, Pillon MC, Thevakumaran N, Sun Y, Chakrabartty A, Guarné A, Kurinov I, Durocher D, Sicheri F. 2016. Structural and functional characterization of KEOPS dimerization by Pcc1 and its role in t^6A biosynthesis. *Nucleic Acids Res* **44:** 6971–6980.

Weissenbach J, Grosjean H. 1981. Effect of threonylcarbamoyl modification (t^6A) in yeast tRNA Arg III on codon-anticodon and anticodon-anticodon interactions. A thermodynamic and kinetic evaluation. *Eur J Biochem* **116:** 207–213.

Winn MD, Murshudov GN, Papiz MZ. 2003. Macromolecular TLS refinement in REFMAC at moderate resolutions. *Methods Enzymol* **374:** 300–321.

Winn MD, Ballard CC, Cowtan KD, Dodson EJ, Emsley P, Evans PR, Keegan RM, Krissinel EB, Leslie AGW, McCoy A, et al. 2011. Overview of the CCP4 suite and current developments. *Acta Crystallogr D Biol Crystallogr* **67:** 235–242.

Yarian C, Townsend H, Czestkowski W, Sochacka E, Malkiewicz AJ, Guenther R, Miskiewicz A, Agris PF. 2002. Accurate translation of the genetic code depends on tRNA modified nucleosides. *J Biol Chem* **277:** 16391–16395.

Zhang W, Collinet B, Graille M, Daugeron MC, Lazar N, Libri D, Durand D, van Tilbeurgh H. 2015a. Crystal structures of the Gon7/Pcc1 and Bud32/Cgi121 complexes provide a model for the complete yeast KEOPS complex. *Nucleic Acids Res* **43:** 3358–3372.

Zhang W, Collinet B, Perrochia L, Durand D, van Tilbeurgh H. 2015b. The ATP-mediated formation of the YgjD–YeaZ–YjeE complex is required for the biosynthesis of tRNA t^6A in *Escherichia coli*. *Nucleic Acids Res* **43:** 1804–1817.